Chapter 7

Vertical wind speed profiles in atmospheric boundary layer flows

Sukanta Basu
Faculty of Civil Engineering and Geosciences, Delft University of Technology, Delft, the Netherlands

7.1 Introduction

The vertical profile of wind speed, extending up to a few hundreds of meters above ground or sea level, is a critical meteorological variable for several application arenas, including (but not limited to) wind resource assessments [1,2], wind engineering [3,4], air pollutant dispersion [5,6], aviation [7], and bird migration studies [8]. Such profiles are typically measured by tall meteorological masts, sodars, lidars, wind profilers, aircraft, balloons, and kites [9–13]. Given the high cost of the instruments/infrastructures and other logistical issues, in general, there is a dearth of tall wind profile measurements around the world. In the absence of observational wind data, high-resolution atmospheric models (e.g., mesoscale models) are often utilized to generate synthetic wind data. Even though this numerical approach has been showing significant promise, there is room for improvement in terms of increasing the accuracy and reliability of the simulated wind data. In the absence of either observed or reliable atmospheric model-generated wind profiles, a wide range of similarity theory-based and empirical equations of varying complexity have been proposed as viable alternatives for wind profile estimations. These equations utilize near ground/sea level wind data (either measured by automated weather stations, mesonets, ocean buoys, or estimated via satellite remote-sensing) and other ancillary data to estimate winds at higher altitudes.

In this chapter, we first provide some examples of vertical wind speed profiles based on field observations from around the world. These examples provide a glimpse into the diversity of wind speed profiles in our atmosphere. Next, we discuss various similarity theory-based and empirical wind profile equations. None of these profiles are generic in nature; rather they are only applicable for specific atmospheric conditions (e.g., neutral stability), suitable for specific locations (e.g., surface layer), or only valid for certain phenomena (e.g., hurricane). Throughout this chapter, we provide numerous illustrative examples from offshore wind energy literature.

7.2 Diversity of wind speed profiles

Wind speed profiles in the atmospheric boundary layer (ABL; the lowest part of our atmosphere) exhibit a myriad of shapes. Sometimes the profiles are approximately logarithmic in nature; other times they can portray somewhat linear trends. There are specific meteorological conditions when wind speeds are more-or-less uniform with height. Certain other conditions can promote "jet" shapes with low-level wind maxima. Some of these shapes can be seen in Fig. 7.1.

The well-known "Leipzig wind profile" is shown in the left panel of Fig. 7.1. The wind data were measured by Mildner [14] using pilot-balloons more than ninety years ago. This specific profile played a pivotal role in early ABL studies (e.g., [15]). Two wind profiles from the well-known Wangara field campaign [16] are documented in the middle and right panels of Fig. 7.1. This campaign was conducted in July and August of 1967 at Hay, Australia [16]. The landscape was flat and almost homogeneous. Given the ideal site condition, the observed wind profiles and other meteorological data have been used for model validation over the years (see [17] and the references therein). The middle panel of Fig. 7.1 represents a daytime unstable condition. Due to strong turbulent mixing, the wind profile is close to being uniform with height. In contrast, the right panel of Fig. 7.1 shows the presence of a low-level jet (LLJ); the nose of the

Wind Energy Engineering. DOI: https://doi.org/10.1016/B978-0-323-99353-1.00031-1

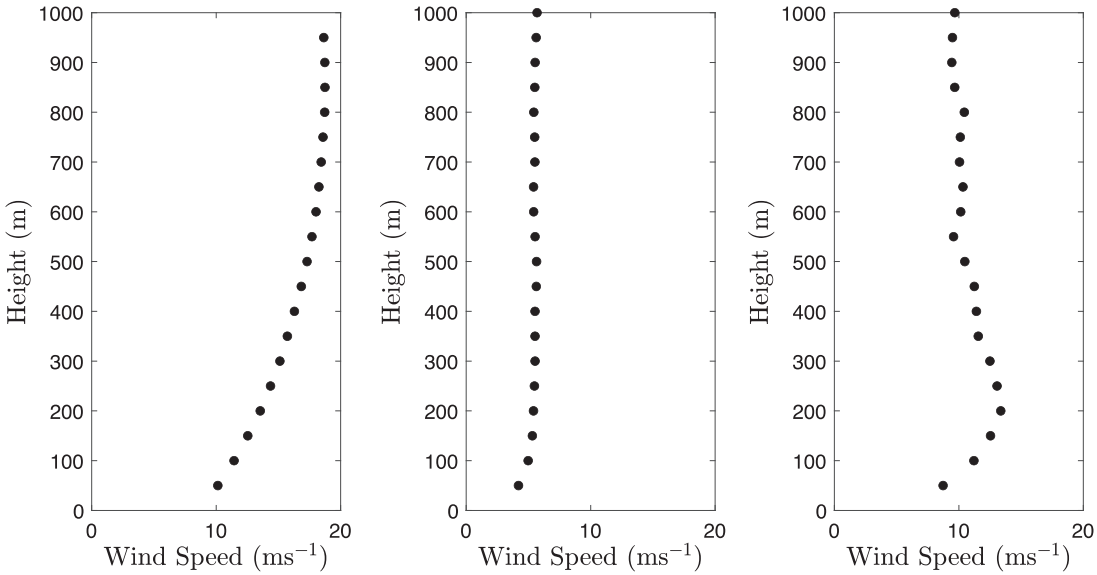

FIGURE 7.1 Observed wind profiles at Leipzig, Germany (*left panel*) and at Wangara, Australia (*middle and right panels*).

LLJ is around 200 m above ground level. This profile was measured during nighttime stably stratified condition. Under such a scenario, turbulent mixing is weak and various atmospheric layers can be partially decoupled from each other and from the underlying surface. As a result, a low-level wind maximum can form; the physical mechanism associated with this phenomenon is called inertial oscillation. More information on LLJs can be found in standard textbooks of ABL (e.g., [18,19]).

A few years ago, Peña et al. [20] attempted to identify canonical wind profiles measured at a coastal onshore location in Denmark. Based on visual inspection, they identified ten different shapes from an extensive observational database composed of sonic anemometers and lidar measurements. Instead of laborious manual identification, Durán et al. [21] proposed an automated wind profile classification approach by using self-organizing feature maps [22]. The readers are encouraged to peruse Peña et al. [20] and Durán et al. [21] to appreciate the diversity of wind profiles.

At present, only atmospheric models [23] with appropriate physical parameterizations [24] have the ability to capture the rich diversity of wind profiles. However, these models are computationally expensive and often suffer from different biases and errors. Instead, for certain applications, one can make use of similarity theory-based and/or empirical equations. In the following section, we delve into various types of similarity theories.

7.3 Similarity theory

Arya [5] defined similarity theory in a succinct manner:

> *A similarity theory, based on dimensional analysis, provides a means of grouping the variables into some dimensionless similarity parameters and organizing the experimental data in the most efficient manner to derive universal similarity relationships.*

In the ABL literature, a wide range of similarity theories have been proposed over the past century (see [9,18,19]). We only discuss the ones which are relevant for wind energy applications.

7.3.1 Logarithmic law of the wall

The logarithmic law of the wall (henceforth Π_{LOG}) is quite often used in wind energy applications:

$$U = \frac{u_*}{\kappa} \ln\left(\frac{z}{z_\circ}\right), \tag{7.1}$$

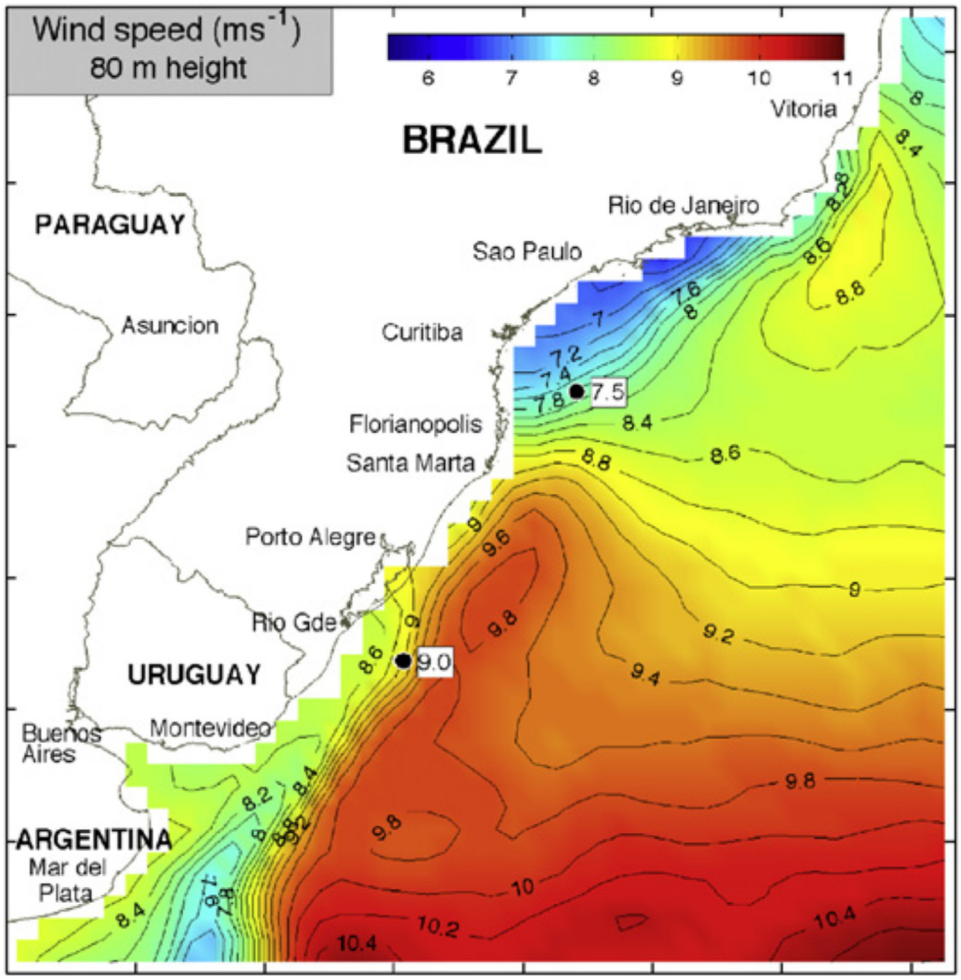

FIGURE 7.2 Offshore wind resource map of southeastern Brazil. This map was created by extrapolating QuikSCAT wind data using Π_{LOG} with $z_\circ = 0.2$ mm. Dates: August 1999–June 2007. *Reproduced with permission from Pimenta F, Kemptona W, Garvinea R. Combining meteorological stations and satellite data to evaluate the offshore wind power resource of Southeastern Brazil. Renew Energy 2008;33:2375–87.*

where $z_\circ$ is the so-called aerodynamic roughness length. Surface friction velocity is represented by u_*. von Kármán constant is denoted by κ. Eq. (7.1) could be re-written as follows:

$$\frac{U_H}{U_r} = \frac{\ln\left(\frac{H}{z_\circ}\right)}{\ln\left(\frac{z_r}{z_\circ}\right)}, \tag{7.2}$$

where U_r is the reference (or measured) wind speed at a given height (z_r), U_H is the estimated wind speed at hub-height (H).

Π_{LOG} has a firm physical basis. It can be derived by a dimensional analysis as well as by more formal approaches (e.g., Millikan's approach). In theory, Π_{LOG} is only applicable in the surface layer[1] for neutrally stratified atmospheric conditions (the regime where the buoyancy effects are virtually insignificant). However, in various wind resource assessment projects, Π_{LOG} has been (quite inappropriately) utilized for the extrapolation of nonneutral (aka diabatic) wind speed profiles.

For example, Pimenta et al. [25] created an offshore wind map ($H = 80$m) of southeastern Brazil by extrapolating satellite remote-sensing (QuikSCAT)-based wind data using Π_{LOG} (Fig. 7.2). Even though this wind map shows heterogeneous spatial distribution of wind speeds, the omission of atmospheric stability makes this wind map less than useful.

1. The lowest part of the ABL is called the surface layer. In this layer, the Coriolis effects can be neglected. Turbulent fluxes of momentum, heat, moisture, and other scalars are assumed to be invariant with height in the surface layer.

7.3.2 Monin−Obukhov similarity theory

Differentiating Eq. (7.1) with respect to z leads to the following equation:

$$\left(\frac{\kappa z}{u_*}\right)\left(\frac{\partial U}{\partial z}\right) = 1. \tag{7.3}$$

This equation is only valid for neutrally stratified conditions. For nonneutral cases, based on dimensional analysis, Monin and Obukhov [26] hypothesized that:

$$\left(\frac{\kappa z}{u_*}\right)\left(\frac{\partial U}{\partial z}\right) = \phi_m\left(\frac{z}{L}\right), \tag{7.4}$$

where L is the Obukhov length [18,19]. The ratio z/L is called the stability parameter (ζ). The function ϕ_m is commonly known as the gradient stability function. By definition, $\phi_m(0)$ equals to 1 (neutral condition).

The exact form of $\phi_m\left(\frac{z}{L}\right)$ cannot be derived solely based on a dimensional analysis; rather, observational (or simulated by high-fidelity models) datasets are needed to derive these functions. In the literature, numerous $\phi_m\left(\frac{z}{L}\right)$ functions have been proposed; please refer to Table 3 of Ref. [27] for some examples.

Eq. (7.4) can be integrated to yield:

$$U = \frac{u_*}{k}\left[\ln\left(\frac{z}{z_\circ}\right) - \psi_m\left(\frac{z}{L}, \frac{z_\circ}{L}\right)\right], \tag{7.5}$$

where $\psi_m\left(\frac{z}{L}, \frac{z_\circ}{L}\right) = \int_{z_\circ/L}^{z/L} \frac{1-\phi_m(\zeta)}{\zeta} d\zeta$ and $\zeta = \frac{z}{L}$. The function ψ_m is widely known as the stability correction term. In this chapter, Eq. (7.5) will be referred to as Π_{MO}. It can be re-written as follows:

$$\frac{U_H}{U_r} = \frac{\ln\left(\frac{H}{z_\circ}\right) - \psi_m\left(\frac{H}{L}, \frac{z_\circ}{L}\right)}{\ln\left(\frac{z_r}{z_\circ}\right) - \psi_m\left(\frac{z_r}{L}, \frac{z_\circ}{L}\right)}. \tag{7.6}$$

Since $z_\circ \ll z_r < H$, it is a common practice to neglect the effect of roughness in the stability correction terms. In other words, Eq. (7.6) can be simplified to:

$$\frac{U_H}{U_r} = \frac{\ln\left(\frac{H}{z_\circ}\right) - \psi_m\left(\frac{H}{L}\right)}{\ln\left(\frac{z_r}{z_\circ}\right) - \psi_m\left(\frac{z_r}{L}\right)}. \tag{7.7}$$

By convention, the stability correction terms (ψ_m) are "subtracted" from the log-law. Thus, with respect to the neutral condition, the wind speeds are supposed to increase (decrease) for stable (unstable) conditions. Several formulations for ψ_m exists in the literature akin to ϕ_m functions. For example, Barthelmie [28] and Holtslag et al. [29] utilized the so-called Businger-Dyer correction terms [30−32]:

$$\psi_m = -\frac{5z}{L}; \text{for} \frac{z}{L} \geq 0 \tag{7.8a}$$

$$\psi_m = 2\ln\left(\frac{1+x}{2}\right) + \ln\left(\frac{1+x^2}{2}\right) - 2\tan^{-1}x + \frac{\pi}{2}; \quad \text{for } \frac{z}{L} \leq 0 \tag{7.8b}$$

where

$$x = \left(1 - \frac{16z}{L}\right)^{1/4}.$$

It should be noted that Monin-Obukhov Similarity Theory (MOST, Π_{MO}) is strictly valid in the surface layer. For typical stably stratified conditions (i.e., $\frac{z}{L} \geq 0$), hub-heights of 100−150 m are much higher than the top of the surface layer. Under this scenario, the applicability of Π_{MO}, Eqs. (7.4−7.7), is highly questionable.

Holtslag et al. [29] analyzed offshore wind data from the Ijmuiden tower in the North Sea (close to the Dutch coastline). They plotted the ratio U_{92}/U_{58} as a function of the stability parameter (z/L); see Fig. 7.3. In addition to the

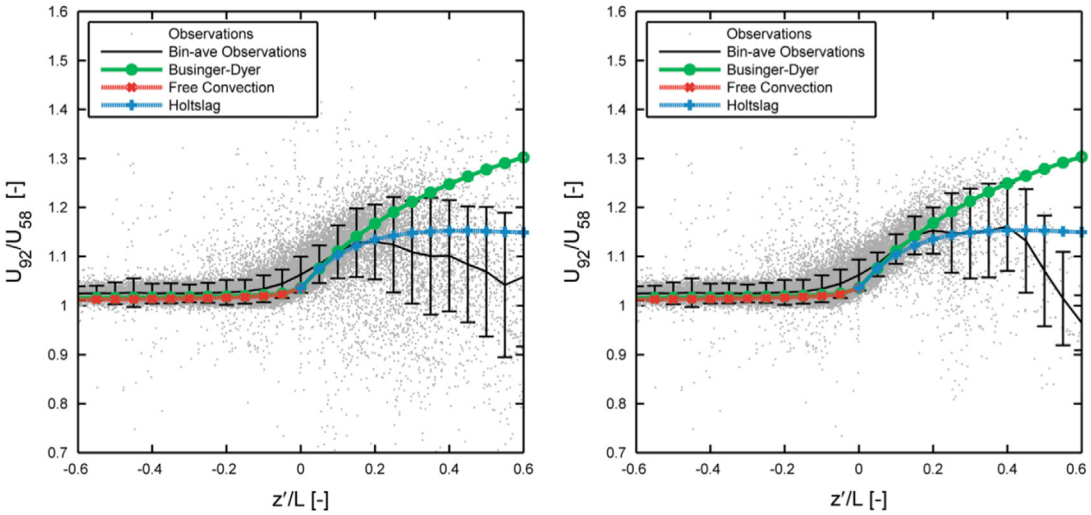

FIGURE 7.3 *Left panel*: the ratio of wind speeds at 92 and 58 m as a function of the stability parameter. Observational data from the IJmuiden tower were used for making this plot. Several empirical formulations (e.g., Businger-Dyer functions) for wind shear are overlaid for direct comparison. *Right panel*: same as left panel; except, filtered data are used in this plot. Basically, for stable conditions, cases with $u_* < 0.2$ m/s were removed. In these plots, $z' = 13.5$ m. *Reproduced with permission from Holtslag MC, Bierbooms WAAM, van Bussel GJW. Validation of surface layer similarity theory to describe far offshore marine conditions in the Dutch North Sea in scope of wind energy research. J Wind Eng Ind Aerodyn 2015;136:180–91.*

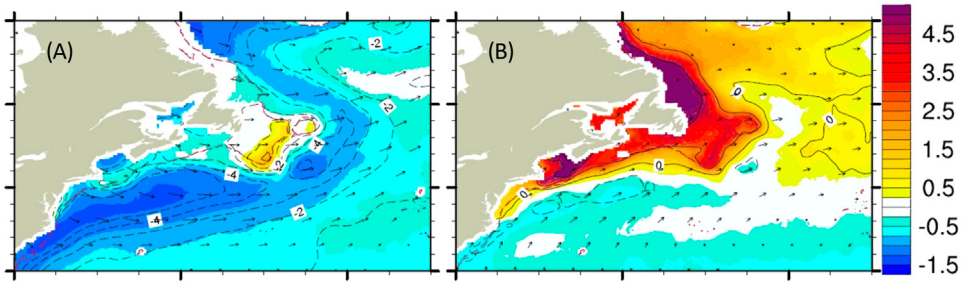

FIGURE 7.4 Π_{MO}-based 80 m wind speed minus Π_{LOG}-based 80 m wind speed (m/s). (A) The winter months (DJF) of 2000–06. (B) The summer months (JJA) of 2000–06. *Reproduced with permission from Capps SB, Zender CS. Global ocean wind power sensitivity to surface layer stability. Geophys Res Lett 2009;36:L09801.*

Businger-Dyer functions [i.e., Eqs. (7.8a) and (7.8b)], they overlaid other empirical stability correction formulations. For example, the ψ_m function proposed by Beljaars and Holtslag [33] was invoked. Based on Fig. 7.3, one can conclude that for unstable conditions, the scatter of the observed data is marginal. More importantly, all the empirical formulations are more-or-less in-line with the observations. However, for stable conditions, the scatter increases tremendously. The empirical formulations performed reasonably well for weakly stable conditions; however, they were not able to capture the observed decrease of wind shear for very stable conditions.

Capps and Zender [34] compared Π_{LOG} and Π_{MO} for the estimation of the global ocean wind energy at 80 m above sea level. They used QuikSCAT-based 10 m wind data and other data sources (e.g., NCEP-DOE AMIP-II Reanalysis). In Fig. 7.4, $U(80\text{m})_{\Pi_{MO}} - U(80\text{m})_{\Pi_{LOG}}$ values are shown for eastern North America. The extrapolated wind profiles are nearly logarithmic during the winter months (*left panel*). However, during the summer months, when stability effects are generally more important, Π_{LOG} underestimates the 80 m wind speed values substantially (3 m/s or more) in extended regions. This figure clearly underscores the need for stability correction functions in the extrapolation methodologies, which have been historically neglected in wind resource estimation projects.

7.3.3 Extension of Monin–Obukhov similarity theory

As mentioned earlier, MOST is strictly valid in the surface layer. Gryning et al. [35] extended the MOST-based wind profiles for the entire boundary layer. In conventional MOST, only a surface layer length scale (l_S) is involved. Gryning et al. [35] hypothesized that an integrated length scale (l) for the entire boundary layer can be written as:

$$\frac{1}{l} = \frac{1}{l_S} + \frac{1}{l_M} + \frac{1}{l_U}; \tag{7.9}$$

where l_M and l_U represent middle and upper boundary layer length scales, respectively. For neutral conditions, they assumed $l_S = z$ and $l_U = (h - z)$; where the variable h denotes boundary layer height. For nonneutral conditions, they followed the MOST prescription of $l_S = \frac{z}{\phi_m}$; where, ϕ_m is the gradient stability function described earlier.

Gryning et al. [35] made another crucial assumption regarding the dependency of friction velocity (u_*) with height; for simplicity, they assumed that u_* decreases linearly with height and goes to zero at the top of the boundary layer. With all these assumptions, they arrived at the following equations for wind speed profiles for different stability conditions (see also [36]):

$$U = \frac{u_*}{\kappa}\left[\ln\left(\frac{z}{z_0}\right) + \frac{z}{l_M} - \frac{z}{h}\left(\frac{z}{2l_M}\right)\right]; \text{for} \frac{z}{L} = 0 \tag{7.10a}$$

$$U = \frac{u_*}{\kappa}\left[\ln\left(\frac{z}{z_0}\right) - \psi_m\left(\frac{z}{L}\right)\left(1 - \frac{z}{2h}\right) + \frac{z}{l_M} - \frac{z}{h}\left(\frac{z}{2l_M}\right)\right]; \text{for} \frac{z}{L} < 0 \tag{7.10b}$$

$$U = \frac{u_*}{\kappa}\left[\ln\left(\frac{z}{z_0}\right) - \psi_m\left(\frac{z}{L}\right) + \frac{z}{l_M} - \frac{z}{h}\left(\frac{z}{2l_M}\right)\right]; \text{for} \frac{z}{L} > 0 \tag{7.10c}$$

Collectively, these wind speed profile equations are termed as Π_{MOX} in this chapter. The stability correction terms (ψ_m) were discussed in the context of Π_{MO}. Identical formulations are also used by [35]. However, in contrast to Π_{MO}, the Π_{MOX} equations require additional parameterizations for h and l_M. Please refer to [35] for further technical details.

Sathe et al. [36] analyzed observational data from a 116 m tall meteorological mast near the Egmond aan Zee offshore wind farm (OWEZ), the Netherlands. They compared Π_{MO} and Π_{MOX} for the OWEZ case under a range of stably stratified conditions (see Table 7.1). Given the complexity of the l_M parameterization in Π_{MOX}, they also explored a slightly simplified formulation in which the length scale l_M is neglected. From Table 7.1, it is evident that Π_{MO} performs quite poorly in the case of very stable condition at upper elevations (i.e., at 70 m and 116 m). The Π_{MOX} formulation with or without l_M performs much better for these scenarios. In the case of near-neutral stability, the performances of Π_{MO} and Π_{MOX} are nearly identical.

We would like to note that Sathe et al. [36] used Businger-Dyer's ψ_m functions [i.e., Eqs. (7.8a) and (7.8b)] in their study. It will be worthwhile revisiting their study with a diverse suite of ψ_m parameterizations (e.g., [33]) in conjunction with Π_{MO}.

TABLE 7.1 Root mean squared error (m/s) between observed and various extrapolated wind profiles.

	21 m	70 m	116 m
Near-neutral stable			
Π_{MO}	0	1.47	2.66
Π_{MOX}	0.02	1.46	2.62
Π_{MOX}, neglecting l_M	0.03	1.47	2.62
Stable			
Π_{MO}	0	2.36	5.71
Π_{MOX}	0.08	2.50	4.35
Π_{MOX}, neglecting l_M	0.03	2.62	4.39
Very stable			
Π_{MO}	0	8.48	21.97
Π_{MOX}	0.48	5.91	9.22
Π_{MOX}, neglecting l_M	0.62	6.06	9.24

Observational data from OWEZ in the wind sector of 225–315 degrees are utilized here.
Source: Sathe A, Gryning S-E, Peña A. Comparison of the atmospheric stability and wind profiles at two wind farm sites over a long marine fetch in the North Sea. Wind Energy 2011;14:767–80.

7.3.4 Geostrophic drag laws

Following the seminal work by Kazanski and Monin [37], various wind profile relationships were proposed in the atmospheric science literature [38–40]. These relationships make use of various boundary layer scaling hypotheses and are collectively known as geostrophic drag laws (Π_{GDL}). In principle, they are applicable in the outer part of the ABL (i.e., above the surface layer) and asymptotically match with Π_{MO} in the surface layer. Unfortunately, due to the lack of reliable high-altitude wind data, Π_{GDL} formulations have not been properly validated and their accuracy remains questionable. Furthermore, their usage requires the availability of different meteorological variables as input: geostrophic wind speed, boundary layer height, Brunt-Väisälä frequency, Obukhov length, friction velocity, roughness length, and Coriolis parameter. Since some of these variables are not routinely available, it is not surprising that Π_{GDL} formulations have not been popular in practical applications (including wind energy). In this respect, the papers by Cvitan et al. [41] and Emeis [42] are worth mentioning as they utilize simplified versions of Π_{GDL} formulations.

7.4 Empirical formulations

In parallel to the development of various similarity theories, a number of empirical formulations of wind speed profiles have been proposed in the literature. In this section, we summarize a few of them.

7.4.1 Power law

Even though Π_{LOG}, Π_{MO}, and Π_{MOX} formulations have been used by the wind energy industry, they are much less popular than the following power-law relationship (Π_{PL}):

$$\frac{U_H}{U_r} = \left(\frac{H}{z_r}\right)^{\alpha}; \tag{7.11}$$

Here α is the so-called shear exponent or the Hellmann exponent [43]. If a reference wind speed is available (e.g., from an ocean buoy), the only unknown in Eq. (7.11) is α. It is well-established in the literature that α strongly varies with atmospheric stability and surface roughness [44–47]. Thus, α is expected to exhibit diurnal, seasonal, and interannual variations. The value of α may also depend on advection and nonequilibrium conditions, which are common in the coastal zone. Nevertheless, constant values of α are often used in wind energy projects. Without any doubt, $\alpha = 1/7$ or 0.14 is the most commonly used value in wind resource estimations. Please note that $\alpha = 1/7$ does not have any physical basis for turbulent boundary layers. It is empirically estimated and has been found to approximately hold under near-neutral conditions over flat terrains with low roughness [43].

Intuitively, a parameterization for α which reliably takes into account the effects of atmospheric stability and surface roughness should yield an improvement over the traditional constant α-based extrapolation approach. Keeping this in mind, Hsu [48] created a simple lookup table for α (Table 7.2) based on a field study on the flat southern coast of St. Croix, U. S. Virgin Islands. To the best of our knowledge, the errors and uncertainties associated with this lookup table for other locations have never been evaluated.

Instead of using the aforementioned lookup table and/or other ad-hoc parameterizations, a far better option is to estimate α from near-surface wind data and utilize it in Π_{PL} for vertical extrapolation. For example, if wind speed measurements (U_1 and U_2) corresponding to two observational levels (z_1 and z_2) are available, α can be easily estimated by inverting Eq. (7.11):

$$\alpha = \frac{\ln(U_2/U_1)}{\ln(z_2/z_1)}. \tag{7.12}$$

TABLE 7.2 Approximate values of α as functions of various coastal environments and atmospheric stabilities.

Stability	Offshore waters	Flat, open coast	Towns or cities
Unstable	0.06	0.11	0.27
Neutral	0.10	0.16	0.34
Stable	0.27	0.40	0.60

Source: Hsu SA. Coastal meteorology. San Diego, CA: Academic Press, Inc.; 1988.

However, if more than two levels of wind data are measured, it is statistically more robust to utilize a standard (ordinary least squares-based) linear regression approach between $\ln(U_k)$ and $\ln(z_k)$; where the subscript k refers to different sensor levels. Please note that, in this regression approach, one implicitly assumes that α remains invariant with height which may not be physically very realistic.

Whether Π_{LOG} can be approximated by Π_{PL} was investigated by Sedefian [49] and Emeis [50]. By matching local slopes, it is straightforward to derive:

$$\alpha = \left[\ln\left(\frac{z}{z_\circ}\right)\right]^{-1}. \tag{7.13}$$

Hsu et al. [51] utilized this equation in an offshore setting. If one assumes $z = 10$ m and $z_\circ = 2 \times 10^{-4}$ m (commonly used in offshore wind energy literature, for example, [52]), α becomes approximately equal to 0.09 ($\ll 0.14$).

Corrigan and Matthiesen [53] analyzed offshore wind data taken over lake Erie in Canada. A ZephIR lidar system was deployed between May 2 and June 10 of 2013 to measure wind speeds and directions at heights of 40, 80, 120, 160, and 200 m, respectively. Even though the lidar's sampling frequency was 15 s, Corrigan and Matthiesen [53] averaged the wind data over 10 min intervals to reduce inherent fluctuations and noise. Then, using Eq. (7.12) in conjunction with wind data from the 80 and 200 m levels, they estimated α. The histogram of estimated values is shown in Fig. 7.5. The mean value of α was only 0.09, much smaller than the conventional value of 0.14. They also reported strong dependence of α on the prevalent wind direction.

7.4.2 Profiles for strong winds

In the wind engineering community, the Deaves and Harris equation [54,55] is quite popular. According to this formulation (Π_{DH}):

$$U(z) = \frac{u_*}{\kappa}\left[\ln\left(\frac{z}{z_\circ}\right) + 5.75\left(\frac{z}{h}\right) - 1.88\left(\frac{z}{h}\right)^2 - 1.33\left(\frac{z}{h}\right)^3 + 0.25\left(\frac{z}{h}\right)^4\right]. \tag{7.14}$$

Here h is the ABL height parameterized by $u_*/6f$. The Coriolis parameter is denoted by f. Even though the Π_{DH} formulation was originally proposed for strong wind and neutral condition, it has been used for other meteorological conditions (see [56]).

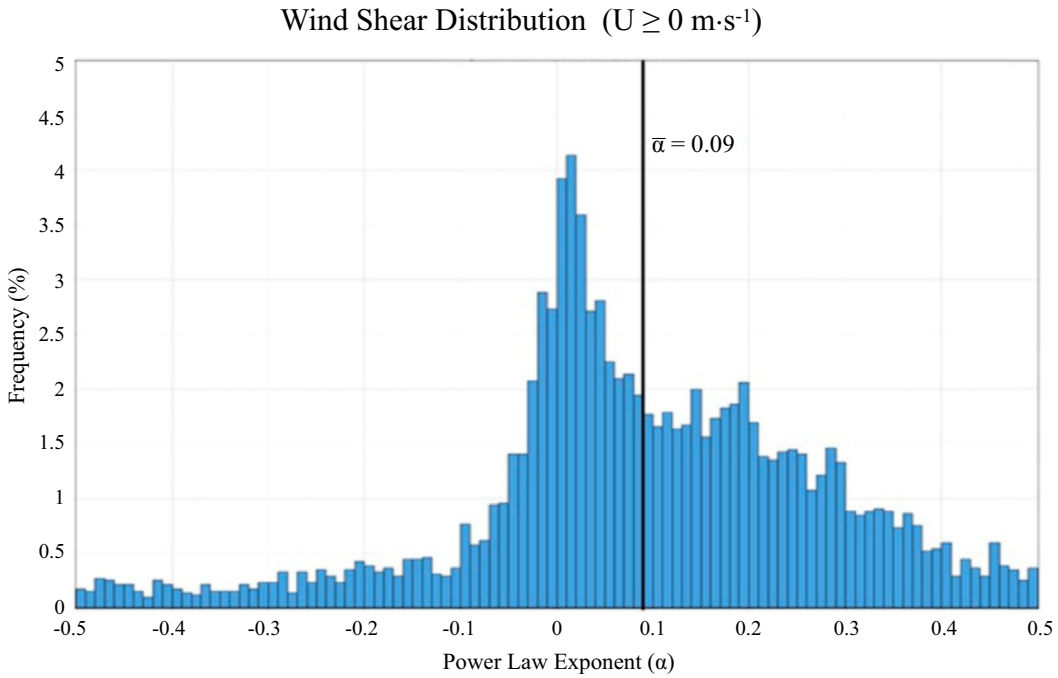

FIGURE 7.5 Histogram of estimated α from wind measurements taken over lake Erie, Canada. *Reproduced with permission from Corrigan D, Matthiesen DH. Analysis of the power law exponent applied to Lake Erie wind shear. Wind Eng 2017;41:103–13.*

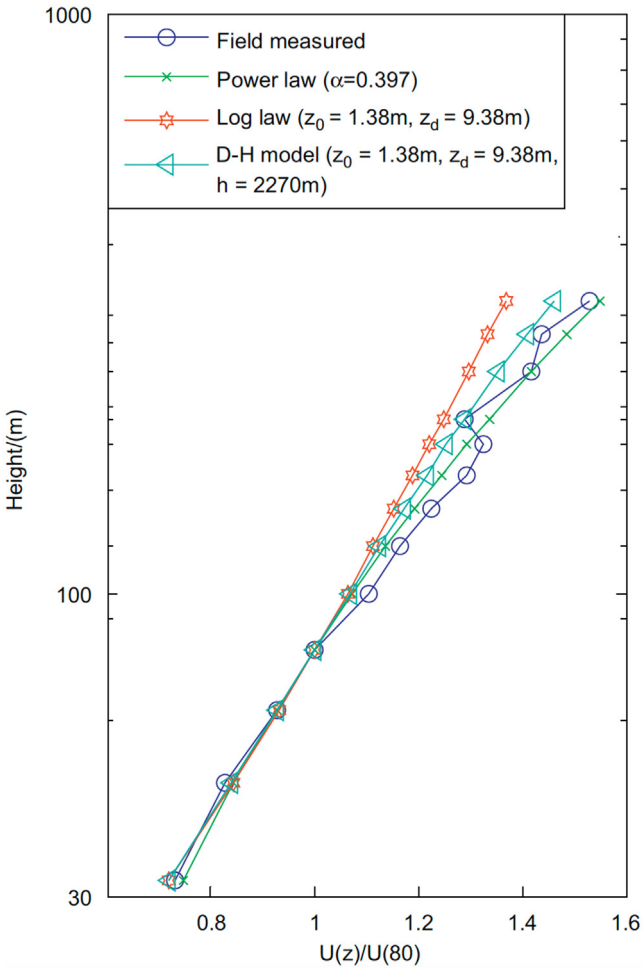

FIGURE 7.6 Comparison of measured and predicted wind speeds during windstorms [57]. *Reproduced with permission from Li Q, Zhi L, Hu F. Boundary layer wind structure from observations on a 325 m tower. J Wind Eng Ind Aerodyn 2010;98:818–32.*

Li et al. [57] analyzed wind data from a 325 m tall tower during twelve windstorms. The measured mean wind speed profile is shown in Fig. 7.6. They compared Π_{LOG}, Π_{PL}, and Π_{DH} against observations. The performance of Π_{PL} and Π_{DH} is comparable. However, Π_{LOG} significantly underestimates the observed wind speeds.

Vickery et al. [58] parameterized wind profiles in hurricanes as follows:

$$U(z) = \frac{u_*}{\kappa}\left[\ln\left(\frac{z}{z_\circ}\right) - a\left(\frac{z}{H^*}\right)^n\right], \tag{7.15}$$

where a and n are free parameters. H^* is the boundary layer height (or jet height) in a hurricane. Recently, an alternate formulation has been proposed by [59]:

$$U(z) = \frac{u_*}{\kappa}\left[\ln\left(\frac{z}{z_\circ}\right) + \eta_0 \sin\left(\frac{z}{H*}\right)\exp\left(-\frac{z}{H*}\right)\right], \tag{7.16}$$

where η_0 is equal to 9.026.

7.5 Concluding remarks

In this chapter, we have discussed various similarity theory-based and empirical wind profile formulations. In terms of model complexity (loosely based on the input data requirements), one can write:

$$\Pi_{PL} \subset \Pi_{LOG} \subset \Pi_{MO} \subset \Pi_{MOX} \subset \Pi_{\mathrm{GDL}}$$

Even though each of these formulations has its own strengths and weaknesses, some of them are clearly more suitable than others for practical applications.

We recommend that the usage of Π_{LOG} should be limited as it is only applicable for neutral conditions; such conditions are rarely present over land and offshore regions. On the same token, Π_{PL} should also not be used with constant α values. As a poor man's approach to account for stability, one can use Π_{PL} with variable α; in this strategy, wind data from the lowest two sensor levels can be utilized to estimate α as a function of time. If more sensor levels are available, one can utilize a more accurate linear regression approach.

Π_{MO} should be utilized for most situations for wind profile estimation within the surface layer. However, the selection of stability correction functions (ψ_m) will be extremely important. For unstable, neutral, and weakly stable conditions, the formulations by Businger and Dyer are adequate. However, for stronger stability conditions, one should experiment with alternative ψ_m formulations.

Π_{MOX} formulation performs better than Π_{MO} for heights above the surface layer. However, Π_{MOX} is much more complicated than Π_{MO} and includes ad-hoc parameterizations (with tuning parameters). Furthermore, by construction, Π_{MOX} cannot be used for heights above the ABL. Thus, for moderately stable and very stable conditions, this approach cannot be used beyond tens of m above the surface.

Arguably, Π_{GDL} are the most suitable formulations for the entire ABL and for a wide range of stability conditions. However, they require numerous inputs and are quite uncertain due to the lack of rigorous validation. With the advent of long-range lidars, reliable high-altitude wind data are becoming more and more readily available. We encourage the wind community to leverage these new datasets and perform comprehensive validation of Π_{MOX} and Π_{GDL} formulations.

Acknowledgments

The author is grateful to Simon Watson and Bert Holtslag for their constructive feedback.

References

[1] Brower MC. Wind resource assessment: a practical guide to developing a wind project. Hoboken, NJ: John Wiley & Sons, Inc; 2012. p. 280.
[2] Emeis S. Wind energy meteorology. Berlin: Springer; 2013. p. 196.
[3] Holmes JD. Wind loading of structures. Taylor & Francis; 2001. p. 379.
[4] Simiu E, Scanlan RH. Wind effects on structures: fundamentals and applications to design. 3rd ed. New York: John Wiley & Sons, Inc; 1996. p. 688.
[5] Arya SP. Air pollution meteorology and dispersion. New York: Oxford University Press, Inc.; 1999. p. 310.
[6] de Visscher A. Air dispersion modeling: foundations and applications. Hoboken, NJ: John Wiley & Sons, Inc; 2014. p. 634.
[7] Lester PF. Turbulence: a new perspective for pilots. Jeppesen Sanderson, Inc.; 1994. p. 290.
[8] Chilson PB, Frick WF, Kelly JF, Liechti F. Aeroecology. Springer; 2017. p. 497.
[9] Sorbjan Z. Structure of the atmospheric boundary layer. Englewood Cliffs, NJ: Prentice Hall; 1989. p. 317.
[10] DeFelice TP. An introduction to meteorological instrumentation and measurement. Upper Saddle River, NJ: Prentice Hall; 1998. p. 229.
[11] Bradley S. Atmospheric acoustic remote sensing. Boca Raton, FL: CRC Press; 2008. p. 271.
[12] Emeis S. Surface-based remote sensing of the atmospheric boundary layer. Springer; 2011. p. 190.
[13] Solari G. Wind science and engineering. Springer; 2019. p. 944.
[14] Mildner P. Über Reibung in einer speziellen Luftmasse. Beitr Phys fr Atmosph 1932;19:151.
[15] Lettau H. A re-examination of the "Leipzig Wind Profile" considering some relations between wind and turbulence in the friction layer. Tellus 1950;2:125–9.
[16] Clarke RH, Dyer AJ, Brook RR, Reid DG, Troup AJ. The Wangara experiment: boundary layer data. Div Meteorol Phys Tech 1971;362.
[17] Basu S, Vinuesa J-F, Swift A. Dynamic LES modeling of a diurnal cycle. J Appl Met Clim 2008;47:1156–74.
[18] Stull RB. An introduction to boundary layer meteorology. Dordrecht, The Netherlands: Kluwer Academic Publishers; 1988. p. 670.
[19] Arya SP. Introduction to micrometeorology. San Diego, California: Academic Press; 2001. p. 420.
[20] Peña A, Floors R, Gryning S-E. The Høvsøre tall wind-profile experiment: a description of wind profile observations in the atmospheric boundary layer. Boundary-Layer Meteorol 2014;150:69–89.
[21] Durán P, Basu S, Meißner C, Adaramola MS. Automated classification of simulated wind field patterns from multiphysics ensemble forecasts. Wind Energy 2020;23:898–914.
[22] Kohonen T. Self-organizing maps. 3rd ed. New York: Springer-Verlag; 2001.
[23] Warner TT. Numerical weather and climate prediction. New York: Cambridge University Press; 2011. p. 526.
[24] Stensrud DJ. Parameterization schemes. New York: Cambridge University Press; 2007. p. 459.

[25] Pimenta F, Kemptona W, Garvinea R. Combining meteorological stations and satellite data to evaluate the offshore wind power resource of Southeastern Brazil. Renew Energy 2008;33:2375–87.
[26] Monin A, Obukhov A. Basic laws of turbulent mixing in the atmosphere near the ground. Tr Akad Nauk SSSR Geo z Inst 1954;24:163–87.
[27] Optis M, Monahan A, Bosveld FC. Limitations and breakdown of Monin-Obukhov similarity theory for wind profile extrapolation under stable stratification. Wind Energy 2016;19:1053–72.
[28] Barthelmie RJ. The effects of atmospheric stability on coastal wind climates. Meteorol Appl 1999;6:39–47.
[29] Holtslag MC, Bierbooms WAAM, van Bussel GJW. Validation of surface layer similarity theory to describe far offshore marine conditions in the Dutch North Sea in scope of wind energy research. J Wind Eng Ind Aerodyn 2015;136:180–91.
[30] Dyer AJ, Hicks BB. Flux-gradient relationships in the constant flux layer. Q J R Meteorol Soc 1970;96:715–21.
[31] Businger JA, Wyngaard JC, Izumi Y, Bradley EF. Flux-profile relationships in the atmospheric boundary layer. J Atmos Sci 1971;28:181–9.
[32] Dyer AJ. A review of flux-profile relationships. Boundary-Layer Meteorol 1974;7:363–72.
[33] Beljaars ACM, Holtslag AAM. Flux parameterization over land surfaces for atmospheric models. J Appl Meteorol 1991;30:327–41.
[34] Capps SB, Zender CS. Global ocean wind power sensitivity to surface layer stability. Geophys Res Lett 2009;36:L09801.
[35] Gryning S-E, Batchvarova E, Brümmer B, Jørgensen H, Larsen S. On the extension of the wind profile over homogeneous terrain beyond the surface boundary layer. Boundary-Layer Meteorol 2007;124:251–68.
[36] Sathe A, Gryning S-E, Peña A. Comparison of the atmospheric stability and wind profiles at two wind farm sites over a long marine fetch in the North Sea. Wind Energy 2011;14:767–80.
[37] Kazanski AB, Monin AS. On the dynamic interaction between the atmosphere and earth's surface. Izv Akad Nauk SSSR, Ser Geofiz 1961;5:514–15.
[38] Blackadar AK, Tennekes H. Asymptotic similarity in neutral barotropic planetary boundary layers. J Atmos Sci 1968;25:1015–20.
[39] Zilitinkevich SS. Velocity profiles, the resistance laws and the dissipation rate of mean flow kinetic energy in a neutrally and stably stratified planetary boundary layer. Boundary-Layer Meteorol 1989;46:367–87.
[40] Zilitinkevich SS, Esau IN. Resistance and heat-transfer laws for stable and neutral planetary boundary layers: old theory advanced and re-evaluated. Quart J Roy Meteorol Soc 2005;131:1863–92.
[41] Cvitan L, Sinik N, Klaić ZB. Two simple wind speed models for practical application under stable conditions. Meteorol Appl 2002;9:423–32.
[42] Emeis S, Baumann-Stanzer K, Piringer M, Kallistratova M, Kouznetsov R, Yuhkov V. Wind and turbulence in the urban boundary layer—analysis from acoustic remote sensing data and fit to analytical relations. Meteorol Z 2007;16:393–406.
[43] Gualtieri G, Secci S. Comparing methods to calculate atmospheric stability dependent wind speed profiles: a case study on coastal location. Renew Energy 2011;36:2189–204.
[44] Frost R. The velocity profile in the lowest 400 feet. Meteorol Mag 1947;76:14–17.
[45] Sisterson DL, Frenzen P. Nocturnal boundary-layer wind maxima and the problem of wind power assessment. Environ Sci Technol 1978;12:218–21.
[46] Irwin J. A theoretical variation of the wind profile power-law exponent as a function of surface roughness and stability. Atmos Environ 1979;13:191–4.
[47] Bañuelos-Ruedas F, Angeles-Camacho C, Rios-Marcuello S. Analysis and validation of the methodology used in the extrapolation of wind speed data at different heights. Renew Sustain Energy Rev 2010;14:2383–91.
[48] Hsu SA. Coastal meteorology. San Diego, CA: Academic Press, Inc.; 1988.
[49] Sedefian L. On the vertical extrapolation of mean wind power density. J Appl Meteorol 1980;19:488–93.
[50] Emeis S. How well does a power law fit to a diabatic boundary-layer wind profile? DEWI Mag 2005;26:59–62.
[51] Hsu SA, Meindl EA, Gilhousen DB. Determining the power-law wind-profile exponent under near-neutral stability conditions at sea. J Appl Meteorol 1994;33:757–65.
[52] Motta M, Barthelmie RJ, Vølund P. The influence of non-logarithmic wind speed profiles on potential power output at Danish offshore sites. Wind Energy 2005;8:219–36.
[53] Corrigan D, Matthiesen DH. Analysis of the power law exponent applied to Lake Erie wind shear. Wind Eng 2017;41:103–13.
[54] Deaves DM, Harris RI. A mathematical model of the structure of strong winds. London: Construction Industry Research and Information Association; 1978. p. 76.
[55] Cook NJ. The Deaves and Harris ABL model applied to heterogeneous terrain. J Wind Eng Ind Aerodyn 1997;66:197–214.
[56] Gualtieri G. Wind resource extrapolating tools for modern multi-MW wind turbines: comparison of the Deaves and Harris model vs. the power law. J Wind Eng Ind Aerodyn 2017;170:107–17.
[57] Li Q, Zhi L, Hu F. Boundary layer wind structure from observations on a 325 m tower. J Wind Eng Ind Aerodyn 2010;98:818–32.
[58] Vickery PJ, Wadhera D, Powell MD, Chen Y. A hurricane boundary layer and wind field model for use in engineering applications. J Appl Meteorol Climatol 2009;48:381–405.
[59] Snaiki R, Wu T. A semi-empirical model for mean wind velocity profile of landfalling hurricane boundary layers. J Wind Eng Ind Aerodyn 2018;180:249–61.